Electronic Supplementary Material (ESI) for Nanoscale.

Supplementary Information Amplitude Nanofriction Spectroscopy

Antoine Lainé[1*], Andrea Vanossi[2,3], Antoine Niguès[1], Erio Tosatti[2,3,4**] and Alessandro Siria[1]

[1] *Laboratoire de Physique de l'École Normale Supérieure, ENS, Université PSL, CNRS, Sorbonne Université, Université Paris-Diderot, Sorbonne Paris Cité, UMR CNRS 8550, 24 Rue Lhomond 75005 Paris, France*

[2] *International School for Advanced Studies (SISSA), Via Bonomea 265, 34136 Trieste, Italy*

[3] *CNR-IOM Democritos National Simulation Center, Via Bonomea 265, 34136, Trieste, Italy*

[4] *The Abdus Salam International Centre for Theoretical Physics (ICTP), Strada Costiera 11, 34151 Trieste, Italy*

[*] antoine.laine@phys.ens.fr

[**] tosatti@sissa.it

Contents

Methods

Tip preparation An electrochemically etched gold tip is glued on the electrode of one prong a the QTF using conductive epoxy. Commercial gold wire from GoodFellow is used. The wire is 200μm thick and of high purity 99.99 %.
Electrochemical etching of the tip is achieved using a double lamellae drop-off technique with Pt electrodes and a $CaCl_2$ solution. A sinusoidal current of amplitude 0.5mA and frequency 10kHz, with a 0.5mA DC offset, is applied through the system. Sharp tips, exhibiting a small bending stiffness, can be further etched in order to obtained blunter tips with a larger bending stiffness. Controlling the shape of the tip enables to eventually control its stiffness in the range $[5 - 500]$ N/m.

HOPG substrate Commercial HOPG substrate from NanoMesh are freshly cleaved just before use and directly installed in the chamber.

Environemental conditions The measurements are performed in a controlled environement avoiding any water and impurity contamination.
Similar results are obtained in a vacuum chamber at pressures of 10^{-6} mbar and 10^{-1} mbar as well as in a Nitrogen satured atmosphere where dessicants are used to remain at a humidity level below 5 %.

Conductance Measurement For all the experiments the bias voltage is imposed on the HOPG substrate while keeping the gold tip grounded. The imposed voltage difference is 13 mV. A current-to-voltage amplifier FEMTO DLPCA 200 is used to amplify the conductance signal. order to create an atomically thin interfacial contact with the HOPG substrate.

S1 Dynamic force measurement

Close to its mechanical resonance, the quartz Tuning Fork (TF) can be modelled as an harmonic oscillator with bare resonance frequency $f_0 \approx 31$ kHz, stiffness $k_{TF} = 40$ kN/m and a quality factor $Q \sim 10^4$ accounting for internal dissipation.
In practice, an external piezo dither implies an input force $F^* = F \cdot e^{i\omega t}$ to mechanically excite the TF and we monitore the resulting prong's displacement $a^*(t) = a_{TF} \cdot e^{(i\omega t + \delta)}$ of the TF. Then we use a Phase-Locked Loop (PLL) and a feedback loop (PID) in order to continuously remain close to the resonance frequency, and at a constant oscillation amplitude. While interacting with an external system, the characteristics of the resonance are modified and the mechanical impedance reads $Z^* = \frac{F^*}{a^*} = \frac{F}{a_{TF}} e^{-i\delta}$ where the real part is the elastic impedance ($Z' = \Re(Z^*)$) and the imaginary part the dissipative impedance ($Z'' = \Im(Z^*)$).

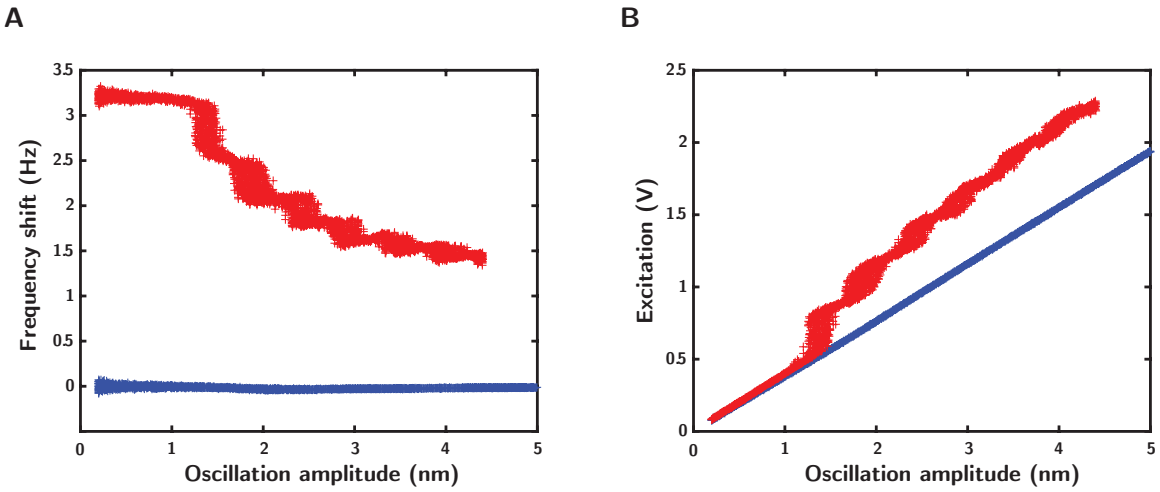

Figure S1: **Raw measurements during an amplitude spectroscopy experiment** Frequency shift **A** and driving excitation **B** of the QTF as a function of oscillation amplitude for the tip in contact with the substrate (red) and out of contact (blue).

Conservative mechanical impedance

The elastic part of the mechanical impedance reads:

$$Z' = 2k_{TF} \cdot \frac{\delta\omega}{\omega_0} \tag{S.1}$$

where $\delta\omega = 2\pi\ \delta f$ relates to the frequency shift.

Dissipative mechanical impedance

The dissipative part of the mechanical impedance is related to the additional force we have to input in the system in order to keep a given oscillation amplitude. $E_{lin}(a_{TF})$ is the input excitation needed to make the resonator oscillate at a given amplitude without interacting with any external system (see blue points in Fig S1 **B**). This linear component is the intrinsic dissipation of the mechanical resonator and is therefore substracted as it does not relate to any physical feature of the system we are interested in

$$Z''(a_{TF}) = \frac{k_{TF}}{Q} \cdot \left(\frac{E(a_{TF})}{E_{lin}(a_{TF})} - 1 \right) \tag{S.2}$$

The dissipative force simply reads $F_D = Z'' \cdot a_{TF}$.

Sampling time: The time of one TF oscillation is $\tau_{TF} = 1/f_0 \approx 30$ μs. The sampling time over which the integration is performed to get one data points is $t_{sampling} = 20$ ms. Then each point is a measurement of an average of $t_{sampling}/\tau_{TF} \approx 650$ TF oscillations.

Amplitude increment rate: The oscillation amplitude is increased at a rate $\frac{da}{dt} \approx 10$ pm.s^{-1}, so $\frac{da}{dt} \approx 3.10^{-4}$ pm/cycle. Thus the time to increase by one substrate periodicity here is about $\frac{\lambda}{da/dt} \approx 25$ s. Considering the system dynamics to be resolved within one TF oscillation $1/f_0 \approx 30$ μs, we have $1/f_0 \ll \frac{\lambda}{da/dt}$ and therefore the system is assumed to evolve in a quasi-static regime.

S2 Harmonically driven PT (HDPT) model

S2.1 Description and computation

PT model We solve the position of the tip $x_{tip}(t)$, with mass m, submitted to a force deriving from a potential $V(x_{tip}, t)$, a dissipative force $m\mu\dot{x}_{tip}$ accounting for phononic and electronic dissipation (for which the characteristic time scale is much slower than the dynamics of the tip position) and a random force due to the thermal excitation of the system $\xi(t)$. The natural frequency of the system reads $\mu_c = 2\sqrt{\frac{K}{m}}$. The dynamics thus follows the Langevin equation [**?**] :

$$m\ddot{x}_{tip} + m\mu\dot{x}_{tip} = -\frac{\partial V(x_{tip}, t)}{\partial x_{tip}} + \xi(t) \tag{S.3}$$

where the potential arising from the interaction with the substrate, and an elastic force due to the TF prong dragging the tip, reads

$$V(x_{tip}, t) = -\frac{U_{\text{eff}}}{2}\cos\left(\frac{2\pi x_{tip}}{\lambda}\right) + \frac{1}{2}K \cdot (x_{TF}(t) - x_{tip})^2 \tag{S.4}$$

with $x_{TF}(t)$ the position of the support, so the position of the prong of the TF.

$$\eta = \frac{2\pi^2 U_{\text{eff}}}{K\lambda^2} \tag{S.5}$$

is a dimensionless parameter evaluating the ratio between the elastic ($\sim K\lambda^2$) and corrugation (U_{eff}) energies. It is reminiscent of the overall dynamics of the system.

Harmonic driving The main difference from conventional PT-based simulation is to input an harmonically driven support position:

$$x_{TF}(t) = a_{TF} \cdot \sin(\omega_0 t) \tag{S.6}$$

as opposed to the classic uniformly driven support. Here the mean support position is fixed. The oscillation frequency is also fixed. By varying the oscillation amplitude a_{TF}, we simultaneously vary the accessible support position as well as the instantaneous velocity $\dot{x}_{TF}(t) = \frac{dx_{TF}}{dt} = a_{TF} \cdot \omega_0 \cdot \cos(\omega_0 t)$.

Computation details We use a 4^{th} order Runge-Kutta algorithm in order to numerically solve the differential equation S.3 with a time step $\delta t = 1$ ns. We solve for the tip dynamics $x_{tip}(t)$ by setting the input parameters $(m, \mu, T, U_{\text{eff}}, K, \lambda)$ and fixing a_{TF}. As we impose the support position $x_{TF}(t)$, we can directly compute the instantaneous force exerted on the spring $F(t) = K \cdot (x_{TF}(t) - x_{tip}(t))$.

Eventually for a given value of a_{TF} we can extract the exact dynamics of the tip in the potential landscape as well as the value of the force at any time. From the force response we can further compute the dissipated energy over one TF cycle by computing the closed loop integral:

$$E_D(a_{TF}) = \oint F(x_{tip})\ dx_{tip} \tag{S.7}$$

From here, we can get the corresponding dissipative force $F_D(a_{TF}) = \frac{E_D(a_{TF})}{4a_{TF}}$ which corresponds to the experimental measurement.

S2.2 Static parameters determination from depinning

The accurate correspondence between the experiments and the matching simulation results allow to extract quantitative estimates of the system parameters.

1. **Stiffness K:** It is obtained from the value of the initial stiffness plateau, before depinning occurs.

2. **Substrate spatial periodicity** λ: It is extracted from the height of the first dissipative step height. Indeed, as depinning occurs $a = a_c$, the dissipation reads $K\lambda$. As we already have an estimate of K, we can access λ. We further confirm this value by observing the friction jump periodicity, which is $\sim \lambda$.

3. **Substrate corrugation U_{eff}:** It is estimated from the depinning amplitude a_c. The static friction is defined as $F_S = Ka_c$. From the PT model, one also has $F_S = \pi U_{\text{eff}}/\lambda$. Thus we can estimated $U_{\text{eff}} = Ka_c\lambda/\pi$.

By definition $\eta = \frac{2\pi^2 U_{\text{eff}}}{K\lambda^2}$ and thus can be estimated experimentally as $\eta = 2\pi\frac{a_c}{\lambda}$ using the above formula.

S3 Turning point thermolubricity

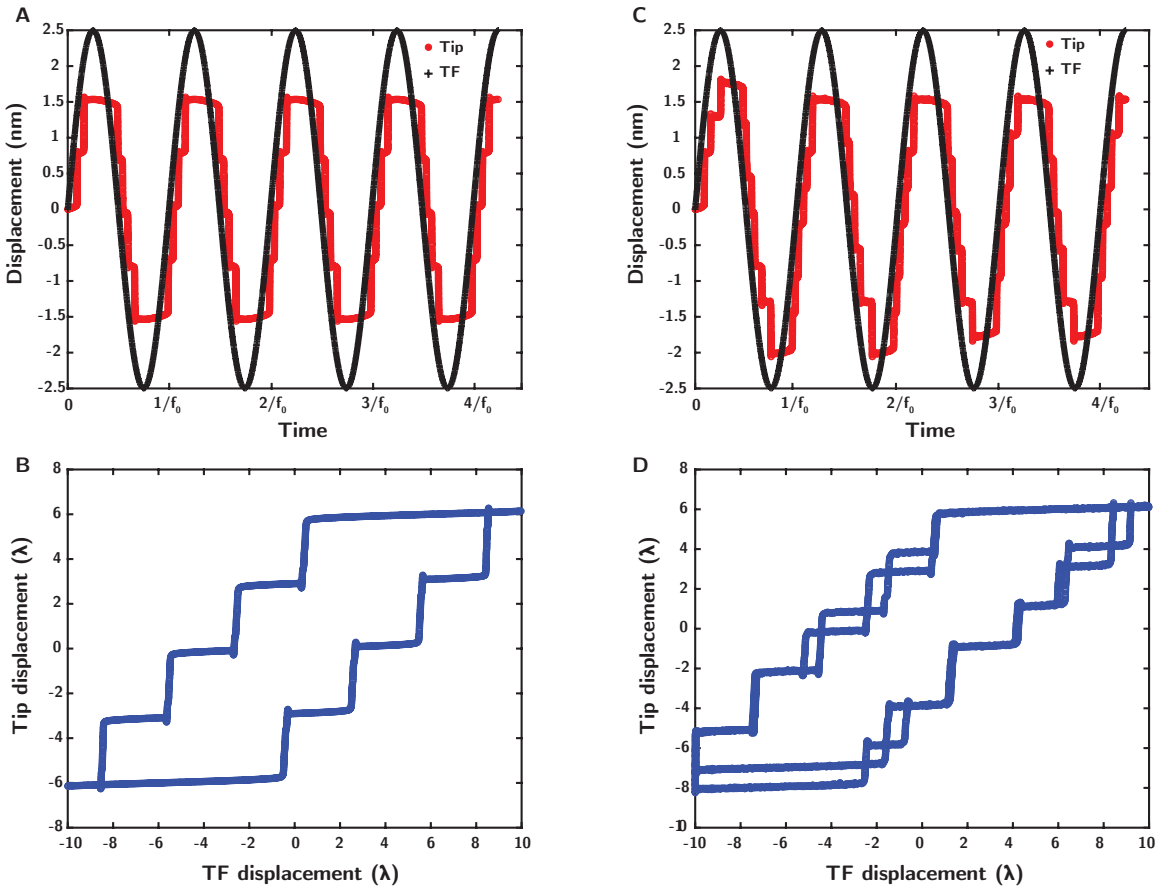

Figure S2: **Thermal effects at the turning point** Tip and TF displacement as a function of time at (**A**) $T = 0$ K and (**C**) $T = 300$ K, for an imposed $a_{TF} = 10\lambda$. Tip displacement as a function of TF displacement for (**B**) $T = 0$ K and (**D**) $T = 300$ K. ($\lambda = 0.25$ nm, $K = 8$ N/m, $U_0 = 9.6$ eV, so $\eta = 60$, $m = 10^{-14}$ kg, $\mu = \Omega_K$.

Fig. S2 presents the impact of the thermal effect on the tip dynamics at the turning points (when the tip velocity changes sign and thus goes by 0). We do observe, from the time response in the $T = 0$ K case (**A**), that the maximum displacement of the tip is of 6λ, corresponding to a displacement 6 potential minima away from the initial one. Here, the dynamics is symmetric and perfectly reproducible in time. Now, in Fig. S2 **B**, the temperature is set to $T = 300$ K and thermal effects appear. We see that at the turning points, the maximum tip displacement is not always the same. It can vary between 6λ, 7λ and 8λ. Thermal hopping events occur at the turning points. The effective potential barrier is decreased due to the spring elongation such that thermal energy becomes capable to overcome it. This thermal hopping events eventually explain the blurring of the force response close to the friction jumps.

S4 Stiffness drop and dissipation increase correlation

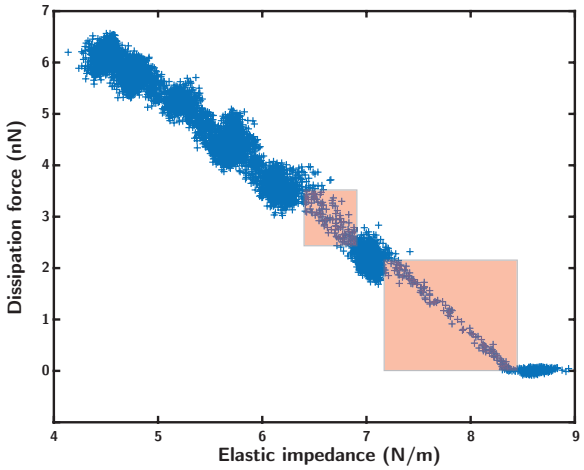

Figure S3: **Coherence within the steps** Experimental data of the dissipative friction force as a function of the average stiffness $\langle Z' \rangle$

We observe, in Fig. S3, a correlation between the dissipation increase and stiffness decrease, for the two first steps (shaded red rectangles).

S5 Stiffness-conductance evolution

Different stiffness contributions The effective stiffness comes as a combination of different stiffnesses acting together. The TF oscillation mode has a stiffness k_{TF}. The tip exhibits a bending stiffness k_{tip} that depends on its shape and constitutive material. Another source of lateral stiffness is due to the contact itself k_c. This last stiffness contribution comes from the elastic displacement of atoms within the substrate and tip with an in-plane elastic shear modulus G^* that gives rise to this contact stiffness. These different contributions, acting in serie, provide

$$\frac{1}{K} = \frac{1}{k_c} + \frac{1}{k_{tip}} + \frac{1}{k_{TF}}$$

Typical values for k_{tip} in AFM experiments lie in the range $1 - 100$ N/m. Typical values for k_c are estimated as $k_c \sim G^* \times r$ with r the typical radius of the contact area. Considering a large (for our case) contact area $r \sim 1$ nm and a shear modulus in the range $G^* \sim 1 - 100$ GPa, we found k_c in the range $\sim 1 - 100$ N/m. As $k_{TF} \approx 40$ kN/m is very large, we can discard any significative impact from this term on the final stiffness measurement. We also consider the tip stiffness to be approximately constant.

Contact area dependence From the initial work [**?**], later confirmed at the nanoscale [**?**], one assumes that the contact stiffness is directly proportional to the contact radius providing $k_c = 8G^*\sqrt{\phi/\pi}$ with G^* the reduced shear modulus of the interface and ϕ the contact area. Following such assumption, the dependence of the total stiffness on the contact area reads:

$$\frac{1}{K} = \frac{1}{k_{tip}} + \frac{\sqrt{\pi}}{8G^*}\frac{1}{\sqrt{\phi}}$$

Fig. S4 shows the inverse of the measured stiffness as a function of the inverse of the conductance square root. The linear fit provides a tip stiffness $k_{tip} \approx 50$ N/m and an effective shear modulus $G^* \approx 64$ GPa (using the Landauer formula to estimate the contact area).

Contact area dependence on the electric conductance In the above discussion, the contact area is estimated using the Landauer formula providing a linear relation between contact area and electric conductance flowing through the contact. Thus assuming the dependence of the contact stiffness on the contact area $k_c \sim \sqrt{\phi}$, it turns out that the linear relation obtained in Fig. S4 evidences the validity of the

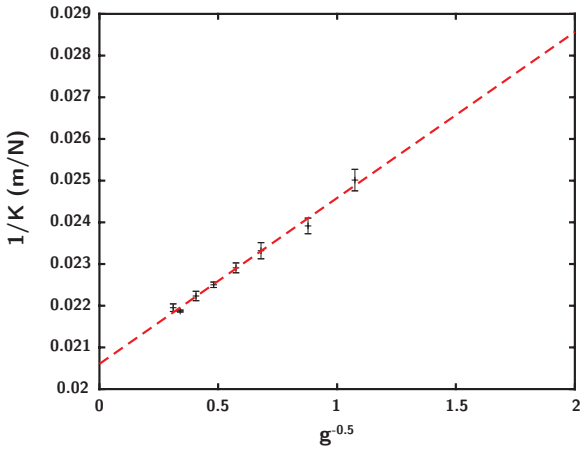

Figure S4: **Contact area - stiffness** Inverse of the effective stiffness as a function of the inverse square root of the conductance.

proportionality between conductance and contact area over the entire conductance range studied.

S6 Large amplitude dissipation from static friction

Fig. S5 shows the typical friction loop for the different tip dynamics regime: largely underdamped **A** and slightly underdamped **B**.

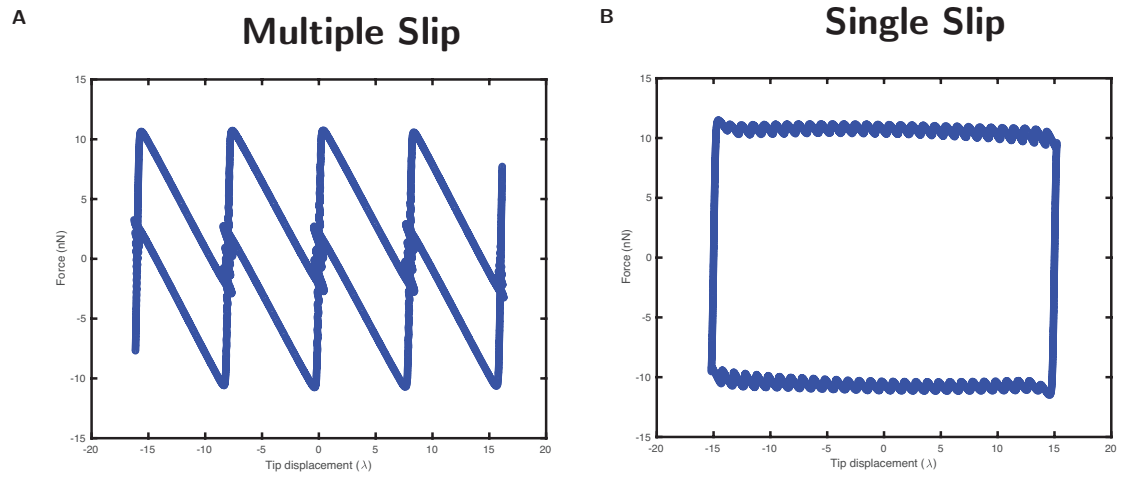

Figure S5: **Friction loop in the different tip dynamics** Numerical results for the instantaneous force $F(t) = K\ (x_{TF} - x_{tip})$ as a function of the tip displacement $x_{TF}(t)$ parametrized by the time t. **A** Multiple slip with $m = 10^{-13}$ kg, $\mu = 0.1\ \mu_c$. **B** Single slip with $m = 10^{-13}$ kg, $\mu = \mu_c$. (Numerical parameters : $\lambda = 0.25$ nm, $T = 0$ K, $K = 8$ N/m, $U_0 = 8$ eV, $a_{TF} = 5$ nm $= 20\lambda$)

Multiple slip: We observe from Fig. S5 **A**, that slip events cover $p = 8$ potential minima in this example, where the tip displacement amplitude reads $a_{tip} \approx 16\lambda$. We define n as the number of slip events during a quarter of an oscillation cycle, thus $np\lambda \sim a_{tip}$.

The loop integral of the friction force is a sum of $4n$ triangles of height F_S and width $p\lambda$. Thus $E_D^{MS} \approx F_S\ p\lambda\ 4n/2$ which simplifies to $E_D^{MS} \approx 2F_S a_{tip}$. Eventually, $F_D^{MS} = E_D^{MS}/(4a_{TF}) \approx \frac{F_S}{2}\ \frac{a_{tip}}{a_{TF}}$.

Single slip: We observe from Fig. S5 **B**, that the loop integral reads $E_D^{SS} \approx 2F_S\ 2a_{tip}$ and we get $F_D^{SS} \approx F_S \cdot \frac{a_{tip}}{a_{TF}}$.

In the end, we find $F_D = \xi F_S$ with $\xi_{1S} = a_{tip}/a_{TF}$ and $\xi_{MS} = a_{tip}/(2a_{TF})$. We observe numerically that $a_{tip} \approx a_{TF}$, for large a_{TF}, thus providing $\xi_{1S} \approx 1$ and $\xi_{MS} \approx 0.5$.